RSC Advances




ROYAL SOCIETY OF CHEMISTRY

www.rsc.org/advances

# Chain entanglement and molecular dynamics of solution-cast PMMA/SMA blend films affected by hydrogen bonding between casting solvents and polymer chains

Yuhua Lv, Yu Lin, Feng Chen, Fang Li, Yonggang Shangguan*, Qiang Zheng

*MOE Key Laboratory of Macromolecular Synthesis and Functionalization, Department of Polymer Science and Engineering, Zhejiang University, Hangzhou 310027,People's Republic of China*

## Abstract:

The effects of intermolecular interaction between casting solvents and polymer chains on molecular entanglement and dynamics in solution-cast poly(methyl methacrylate)/poly(styrene-co-maleic anhydride) (PMMA/SMA) films were investigated by dynamic rheological measurement and broadband dielectric spectroscopy. A series of polymer blend films were cast from the mixed solvents composed of m-xylene and acetic acid with different mass ratio of acetic acid ($R_{ac}$) at a solution concentration of 5 wt%, and in solutions the quantity of hydrogen bonding between PMMA and acetic acid was adjusted by $R_{ac}$. FTIR results confirmed the existence of hydrogen bonding between carbonyl in PMMA and hydroxyl in acetic acid. Although the topological entanglement density of the resultant films decreased with increasing $R_{ac}$, the $\alpha$-relaxation peak shifted towards lower frequency and a higher glass transition temperature ($T_g$) appeared due to the increased cohesional entanglement in PMMA/SMA blend films induced by hydrogen bonding between

* Corresponding authors. Department of Polymer Science and Engineering, Zhejiang University, Hangzhou 310027, PR China. Tel./fax: t86 571 8795 3075. *E-mail addresses:* shangguan@zju.edu.cn

PMMA and acetic acid. Furthermore, the dc conductivity decreased due to the more homogeneous structure in PMMA/SMA blend films cast from mixed solvents with higher $R_{ac}$. Neither the width distribution of $\alpha$-relaxation nor the dynamics of $\beta$-relaxation in these films was influenced by hydrogen bonding between PMMA and acetic acid due to the unchanged heterogeneity of the segmental dynamics and local environment of the segments. These results revealed that the hydrogen bonding between polymers/solvent during casting film can greatly influence the chain entanglement and molecular dynamics of the resultant polymer blends due to the memory effect of polymer chain.

*Key words:* Hydrogen bonding; cohesional entanglement; molecular dynamics

## 1. Introduction

As one of the major routes to prepare uniform, thin and transparent polymer films in many applications, such as painting, coating and adhesives etc, the solution casting technique has aroused general concern in recent decades [1-5]. For the rapid drying process of casting films, the polymer chains do not have enough time to approach the conformational equilibrium before vitrification and consequently the chain conformation in the solution can more or less survive in the resultant films, known as the chain memory effect [6]. Different processes of casting films may result in the distinct architecture structures of macromolecules including conformation, entanglement and packing state of polymer chains, which may influence the

macroscopic properties of the product such as glass transition temperature ($T_g$) [7, 8], polymer chain relaxation [9], phase-separation [5, 10] and crystallization behavior [11, 12]. As a result, many researchers laid their emphasis on the process of solution casting to investigate the relationships between preparing process and macroscopic performance of the solution-cast films [7, 13-18].

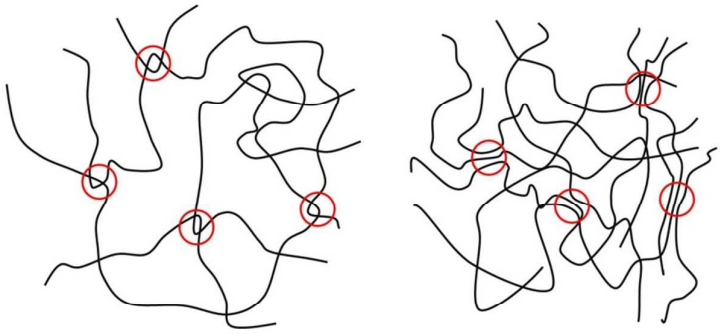


Fig. 1 Schematical of toplogical entanglement and cohesional entanglement.

Reproduced with permission from 1997, Wiley VCH. [27]

Many variables during solution casting process, such as drying rate [7, 13], annealing time [13], solution concentration [14, 15], solvent quality [7, 14, 16] etc, could significantly affect the architecture structures of polymer chain and properties of the resultant films. Li et al. [7] found that rapid drying precluded the polymer chains from achieving full interpenetration before vitrification and some memories of the chain conformation in the solution were held and survived in the resultant films. Usually, in order to ensure complete evaporation of the solvent, the samples are inevitably treated through annealing. Recently, we investigated the influences of annealing on the chain entanglement and molecular dynamics in solution-cast

poly(methyl methacrylate)/poly(styrene-co-maleic anhydride) (PMMA/SMA) blends, and found chain entanglement density increased as the increasing annealing temperature and/or time, leading to higher $T_g$s and longer relaxation time [19]. With regards to the chain entanglement, there are two types of of chain entanglement in amorphous polymer: topological entanglement [20-24] and cohesional entanglement [25-27], as schematically demonstrated in Fig.1. The former comes from the entanglement of different chains in three-dimensional space [20-22], while the latter results from interchain cohesion with local parallel alignment of neighboring segments as physical crosslinks [26, 27]. As to solution concentration, when the casting solution concentration increases, the $T_g$ and relaxation time of the blend film increases due to the more densely packed chain conformation both in the casting solution and the blend films [14]. Besides the solution concentration, the conformation of polymer chains in the solution also strongly depends on the solvent quality [6]. In a good solvent, the intermolecular interaction between polymer segments and solvent is dominant rather than the interaction between segments, which enables the polymer chain to swell. On the contrary, the chains collapse in a poor solvent and as a result, the resultant blend film appears a more compact architecture structure.

In previous report [14], it was found that the PMMA/SMA films cast from a N, N-dimethylformamide (DMF) solution presented higher $T_g$ and longer segmental relaxation time than those of the films cast from chloroform, methyl ethyl ketone and tetrahydrofuran solution. These results were ascribed to the higher entanglement

degree in PMMA/SMA blend films and in turn the decreased segment mobility induced by poor solvent quality of DMF. However, it was noticed that there exists a strong interaction, namely hydrogen bonding between PMMA and DMF in solution [3]. More importantly, the intermolecular interaction between polymer and solvent molecule such as hydrogen bonding can influence the chain conformation in the solution as indicated by some previous reports [3, 28-31]. For example, it was found that poly(vinylidene fluoride-co-hexafluoropropylene) (P(VDF-co-HFP)) membranes with different crystalline phase compositions could be obtained by using acetone and dimethylacetamide (DMAc) due to the different solvent-polymer interactions, and the different solubilities and diffusivities of ethyl acetate (EtAc) in the two solution-cast membranes appeared [28]. On the basis of solvent polarity, a water-soluable conjugated polymer, poly[2,5-bis(diethylaminetetraethylene glycol)phenylene vinylene] (DEATG-PPV) presented a wide range of chain conformations: extended, coiled, and collapsed chain conformations in solutions, leading to distinct morphologies and optical properties in resultant films [30]. Thus, taking the fact that the hydrogen bonding between solvent and polymer can be destroyed during solvent evaporation into account, whether this interaction in the solution influences the architecture structure of the resultant PMMA/SMA film is still unknown, and it is important and necessary to estimate the contribution of this intermolecular interaction to the elevated $T_g$ and increased segmental relaxation time of PMMA/SMA film.

As mentioned above, so far there are many investigations about the effect of solvent quality on performances of solution-cast films [6, 32-36], and the solvent

quality is always represented by the solubility parameter $\delta$. Actually, the $\delta$ criterion representing the interaction between the solvent and polymer can only work reasonably well for non-polar interactions due to van der Waals forces between species, since it results from the Flory interaction parameter $\chi$ and is obtained by the method developed by Hildebrand and Scott [37]. However, it fails in the mixtures with strong polar or specific interactions, such as hydrogen bonds [38]. Thus, how the strong solvent-polymer interaction affects the microstructure and molecular dynamics of the resultant films has not been figured out yet.

As one of the most important interactions between species, hydrogen bonding widely exists in several polymer-solvent systems. In this article, we try to probe whether and how the hydrogen bonding between the solvent and polymer affects the molecular architecture and dynamics of the resultant blend films by using rheological measurement and broadband dielectric spectroscopy. Theorotically, taking pure PMMA as the investigated model would be simpler and more instrutive, yet the solution-casting blend films of PMMA/SMA instead of pure PMMA are chosen as the model system for the following two reasons: firstly, in order to compare the results with the previous publications and keep the continuity of research, we still use the PMMA/SMA system; secondly, the α-relaxation and β-relaxation of pure PMMA will mix to one signal in the investigated temperature, which would lead to erroneous results fitted from dielectric measurments. [39] In order to achieve a good dissolution of the PMMA/SMA blends and control the quantity of hydrogen bonding between polymer/solvent, a series of mixed solvents composed of m-xylene and acetic acid

with different mass ratio of acetic acid ($R_{ac}$) were applied to cast films. The molecular entanglement and dynamics of PMMA/SMA films were investigated by dynamic rheological measurement and broadband dielectric spectroscopy (BDS) to evaluate the effects of hydrogen bonding between polymer/solvent.

## 2. Experimental

### *2.1. Materials and sample preparation*

Polymethyl methacrylate (PMMA, IF850) with $M_w = 8.1\times10^4$ g/mol and $M_w/M_n$ = 1.9 was purchased from LG Co. Ltd, South Korea. Poly (styrene-co-maleic anhydride) (SMA, 210) with $M_w = 2.6\times10^5$ g/mol, $M_w/M_n = 3.7$ and a MA content of 10 wt% was obtained from SINOPEC Shanghai Research Institute of Petrochemical Technology, China. Acetic acid (AR, Shanghai) and m-xylene (CP, Shanghai) were used to prepare a mixed solvent to cast the blend film. The pure m-xylene was also used to cast film as a reference. The parameter $R_{ac}$ was used to represent the mass ratio of acetic acid in the mixed solvent. PMMA/SMA (20/80 wt/wt) blends were dissolved in the mixed solvent ($R_{ac}$ = 0, 0.1, 0.2, 0.4) respectively with a weight concentration of 5% to form a clear and uniform solution. According to the calculated $c^*$(critical overlap concentration) and $c_e$ (entanglement concentration), the 5wt% PMMA/SMA solution is identified to locate in the concentrated regime and the details are demonstrated in Supporting Information. The homogeneous solution was then cast onto a horizontal flat glass Petri dishes held at 35 $^oC$ and dried at 50, 70 and 90 $^oC$ successively in an ordinary oven for at least 3 days. Finally, the films were dried at 110 and 130 $^oC$ in a vacuum oven (vacuum degree < 133 Pa) for 5 days to remove residual solvent. It's

151 convinced by thermogravimetry analysis (Q600, TA, USA) results (as indicated by
152 Fig. S1 in Supporting Information) that the residual solvent had been completely
153 removed. All dried blend films with thickness of 200±10 μm were homogeneous (all
154 samples appear a single glass transition temperature from the broadband dielectric
155 spectroscopy (Fig. 4) and DSC( Fig.5a) method) and optically transparent.

156 *2.2. FTIR spectroscopy*

157 With the evaporation of acetic acid at 25 $^{o}$C, the Fourier Transform Infrared
158 (FTIR) spectrum for the acetic acid solution of PMMA was recorded in the range of
159 4000-400 $cm^{-1}$ on a Fourier transform Infrared Spectroscopy (Nicolet 6700, Thermo
160 Fisher Scientific, USA) with a spectral resolution of 4 $cm^{-1}$. Also the pure acetic acid,
161 the PMMA films cast from acetic acid, m-xylene and their mixed solvents were tested.
162 All the spectra were baseline corrected and automatically smoothed thereafter using
163 Nicolet Omnic.

164 *2.3. BDS spectroscopy*

165 Broadband dielectric spectroscopy (BDS) measurements of PMMA/SMA blend
166 films were conducted on an Alpha high resolution dielectric analyzer (GmbH
167 Concept 40, Novocontrol Technology, Germany), which is equipped with a Novocool
168 cryogenic system for temperature control with a precision of ±0.1 $^{o}$C. The film
169 samples were placed between two circular gold electrodes with a diameter of 20 mm.
170 Temperature sweeps were carried out at a frequency of 10 Hz and a heating rate of 3
171 $^{o}$C/min from 80 to 160 $^{o}$C. Isothermal frequency sweeps were performed over a wide
172 frequency range of $10^{-1}$-$10^{7}$ Hz in the temperature range of 40 - 160 $^{o}$C.

### *2.4. Rheological measurements*

To obtain the samples for rheological measurements, 8 pieces of films with thickness of 200 μm were piled up and compression molded into a specimen disk with a diameter of 25mm and a thickness of 1.5mm at 10MPa and 160°C. In order to minimize the influence of annealing, the hot compression process was completed in 5 min. The rheological measurements were carried out on an advance rheometric expansion system (ARES-G2, TA, USA) with parallel plate geometry of 25 mm in diameter. Frequency sweeps were conducted in the range of 0.01 - 500 rad/s from low to high frequency at 160 °C. The strain amplitude of 1% was employed to ensure all the rheological tests to lie in the linear viscoelastic region (indicated by Fig. S2 in Supporting Information). During these frequency sweeps, the test time required for a point at high frequency is short (a few seconds) while long (hundreds of seconds) at low frequency. Consequently, the full spectra of storage modulus ($G'$) and loss modulus ($G''$) takes about 2 hours from 0.01 rad/s to 500 rad/s and it takes more than 90 min from 0.01 rad/s to 0.1 rad/s. As shown in Fig. S3 in Supporting Information, the increase of $G'$ in the beginning may be ascribed to the influence of hot-compression procedure which also has a annealing effect on smaples indeed besides compressive stress. Considering that the annealing time is very short and all the samples underwent the same process, the equilibrium value of storage modulus will minimize the influence of hot-compression procedure, but the storage modulus obtained in one thousand seconds may contain the contribution of hot-compression procedure or annealing effect.

195 *2.5. MDSC tests*

196 Thermal characteristics of PMMA/SMA blend films were determined with a
197 modulated differential scanning calorimeter(MDSC, Q100, TA, USA). Samples of
198 5-10 mg were used in this test. A heating rate of 2 $^{o}$C/min was employed from 70 $^{o}$C
199 to 140 $^{o}$C with temperature modulation amplitude of 0.5 $^{o}$C and an oscillation period
200 of 60s throughout this investigation. All the tests were run in a nitrogen flow of 50
201 ml/min.

202 ## 3. Results and discussion

203 *3.1.Hydrogen bonding between PMMA and acetic acid*

204 In this article, we try to probe whether and how the hydrogen bonding between
205 solvent/polymer affects the molecular architecture and dynamics of the resultant
206 blend films by using rheological measurement and broadband dielectric spectroscopy.
207 The quantity of hydrogen bonding between polymer and solvent was controlled by
208 changing the mass ratio of acetic acid in the mixed solvents. It is noticed that only the
209 hydrogen bonding between PMMA and acetic acid will be considered, because SMA
210 can't be dissolved at all in acetic acid both at room temperature or heating while it
211 can be completely dissolved in the mixed solvents used in this work. It is widely
212 accepted that hydrogen bonding between the solvent and polymer facilitates the
213 dissolution of polymer in solvent, so the above facts indicates that hydrogen bonding
214 impossibly exists between acetic acid and MA, which may be ascribed to the high
215 rigidity of SMA chains induced by the dominant (90% styrene in SMA) phenyl side
216 chain and in turn a large steric hindrance for the formation of hydrogen bonding

between acetic acid and MA.

Affirming the existence of hydrogen bonding between PMMA and acetic acid during casting PMMA/SMA films is a precondition. FTIR spectra were used to determine the intermolecular interaction between PMMA and acetic acid. To avoid unexpected noise on FTIR spectra and clearly identify it, the casting film process of pure PMMA was chosen. Fig. 2(a) shows the infrared spectra of acetic acid, PMMA/acetic acid solution, and PMMA film cast from acetic acid, respectively. On the PMMA spectrum, the following characteristic peaks appear: the peaks representing the stretching vibration of the C-O-C and C-H at 1300-1100 $cm^{-1}$ and 3000-2840 $cm^{-1}$, respectively; the stretching peak of C=O in carbonyl groups at 1732 $cm^{-1}$; the peaks representing the bend vibration of $-CH_2$ and $-CH_3$ groups at 1442 and 1388 $cm^{-1}$, respectively. On the acetic acid spectrum, several characteristic peaks appear: the stretching vibration peak of -OH at 3300-2500 $cm^{-1}$; the stretching vibration peak of C=O at 1711 $cm^{-1}$ (dimer of acetic acid); the coupling peaks of stretching vibration of C=O and bend vibration of -OH at 1411 $cm^{-1}$ and 1292 $cm^{-1}$; the stretching vibration peak of C-O at 1012 $cm^{-1}$; the out-of-plane bend vibration of –OH and O-H----O at 933 $cm^{-1}$ and 619 $cm^{-1}$, respectively; the in-plane deformation vibration of C-C=O at 478 $cm^{-1}$. Due to the hydrogen bonding between acetic acid molecules, the peak at 3300-2500 $cm^{-1}$ becomes wide. As to the PMMA/acetic acid solution, the characteristic peaks are similar to that of acetic acid, which should be ascribed to the less content of PMMA compared with acetic acid in the initial solution. As a result, most of the characteristic peaks of PMMA are covered by the broad peaks

of acetic acid. In spite of this, the characteristic peaks of PMMA/acetic acid solution at the range of 4000-1300 $cm^{-1}$ are broader compared with that of acetic acid, indicating that there exist interactions between PMMA and acetic acid.

The real-time infrared spectra of a 5 wt% PMMA/acetic acid solution upon volatilizing at 25 $^{o}$C are presented in Fig.2 (b). The four curves presented in Fig.2 (b) correspond to the marked time points (1-4) in the volatilization curve of acetic acid given in Fig. S4 in Supporting Information, respectively. As acetic acid evaporating, the characteristic peaks in Fig.2 (b) become narrower and weaker due to the decrease of acetic acid molecules. Meanwhile, more associated acetic acid molecules are separated to be non-associated ones, which can be proved by the weak peak located at 3558 $cm^{-1}$ indicating the stretching vibration of non-associated -OH in acetic acid. On the other hand, the characteristic peak at 1178 $cm^{-1}$ for PMMA is observed as acetic acid evaporates, meaning that the content of PMMA in the tested sample increases significantly and the acetic acid decreases. Most importantly, one can find that a shoulder peak appears at 1780 $cm^{-1}$ near the stretching vibration peak of C=O at 1732 $cm^{-1}$ and subsequently becomes weaker [3]. It is reasonable to attribute this peak to hydrogen bonding between the carbonyls in PMMA and the hydroxyls of acetic acid. The gradually weaker shoulder peak at 1780 $cm^{-1}$ indicates that the quantity and/or strength of hydrogen bonding between acetic acid and PMMA reduce as the acetic acid decreases.

The similar FTIR results of PMMA films cast from acetic acid, m-xylene and their mixed solvent are presented in Fig.2(c). Since there is no specific intermolecular

interaction between m-xylene and PMMA except van der Waals force, certainly there is no hydrogen bonding in the resultant film from m-xylene. Considering the almost identical FTIR spectra of three films, one can deduce that there is no hydrogen bonding between the solvents and PMMA in all three resultant films. Thermogravimetric analysis (TGA) results given in Fig. S1 in the Supporting Information also confirm that no residual solvent remains in them. In this investigation, the mass ratio of PMMA/SMA blend films taken as the model system is 20/80 in order to investigate the effect of the quantity of hydrogen bonding. The mixed solvents composed of m-xylene and acetic acid with different $R_{ac}$ were used as the casting solvents since the SMA component is insoluble in acetic acid at all. In addition, small portion of acetic acid minimizes the change of solubility parameter of the mixed solvents rather than pure acetic acid. The mixed solvents with different $R_{ac}$ match the PMMA/SMA (20/80) blend well to change the quantity of hydrogen bonding between PMMA chains and acetic acid without an evidently variation of solubility parameter.

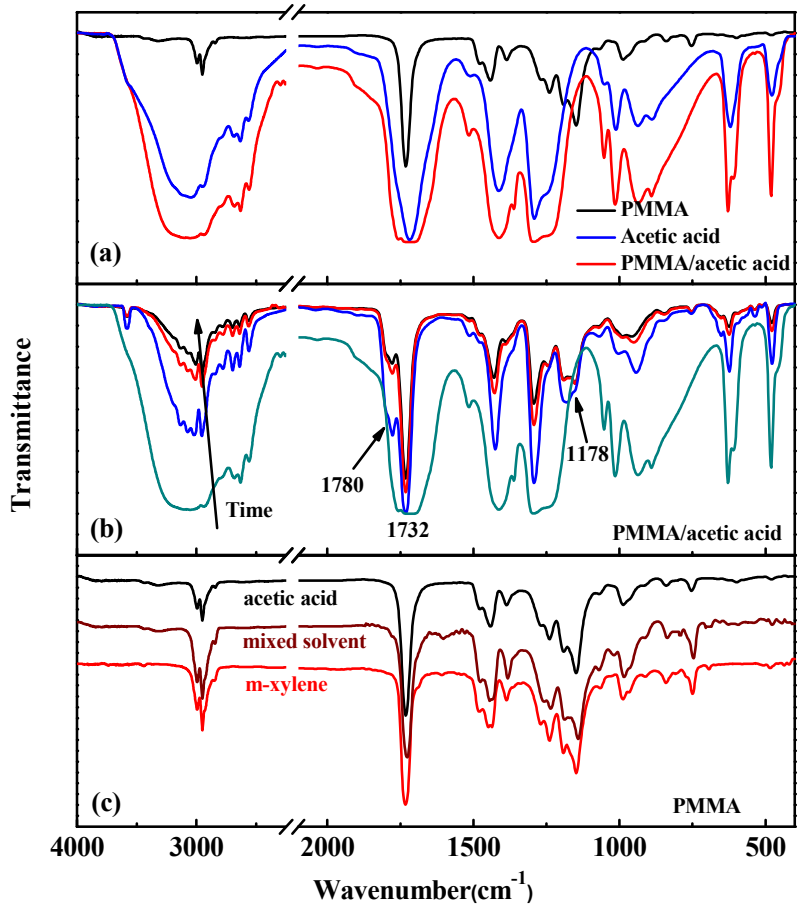


Fig. 2 FTIR spectra of (a) PMMA film cast from acetic acid, acetic acid and PMMA/acetic acid solution, (b) real-time FTIR spectra of PMMA/acetic acid solution as the acetic acid volatilized and (c) PMMA films cast from acetic acid, m-xylene and their mixed solvent, respectively. The four curves in (b) correspond to the time of the marked points (1, 2, 3, 4) in Fig. S4 in Supporting Information.

*3.2.Topological entanglement of molecules*

Since the 5 wt% PMMA/SMA solution used here is in the concentrated regime [14, 40-42], polymer chains entangle with each other. Hence, the chain entanglement density is very important for the properties of the resultant films. As mentioned in the Introduction, there are topological entanglement [20-24] and cohesional entanglement [25-27] in amorphous polymer.Since the topological entanglement can intuitively demonstrate the long chain characteristics of polymers and is easily measured by

experiments compared with cohesional entanglement, it is widely used to describe the architecture structures of polymeric materials. Thus, the topological entanglements of blend films were firstly investigated in this section. Rheological measurments were adopted to obtain parameters related to the topological entanglements. As is shown in the Experimental section, the tested samples were hot-compression molded by the casting PMMA/SMA films at 160$^{o}$C because the 200μm casting films were too thin for the rheological measurements. It must be pointed out that the annealing effect in the hot-compression procedure will affect the storage modulus $G'$ and loss storage $G''$ slightly.(-shown in Fig. S3 in the Supporting Information) Consequently, on one hand, we minimized the time of hot-compression procedure to reduce the annealing effects on the samples; on the other hand, we adopt the same hot-compression process and the same number of layers to ensure the variations of different samples are identical. Based on above reasons, we believed that the comparison between the following results in this work can effectually reflect the influence of hydrogen bonding between casting solvents and polymer chains on the topological entanglements of the resultant PMMA/SMA films.

In our previous study [5, 19], the entanglement molecular weight, $M_e$, defined as the average molecular weight between adjacent temporary entanglement points, can be calculated from the plateau modulus $G_N^0$ (eq.1). By measuring storage modulus $G'$ and loss storage $G''$ in rheological test, $G_N^0$ can be determined by the MIN method (eq.2) [43- 45] and the 'Crossover modulus-based' method (eq.3) [44] respectively,

which is shown in the inlay of Fig. 3 schematically.

$$G_N^0 = \frac{4}{5}\frac{\rho RT}{Me} \quad (1)$$

In which $\rho$ is the density, $R$ is the gas constant, and $T$ is the absolute temperature. In this work, the values of $M_e$ were calculated from $G_N^0$ obtained by the MIN method(eq.2) [43–45] and the 'Crossover modulus-based' method (eq.3)[44] respectively for comparison.

$$G_{N\,exp}^0 = G'(\omega)_{tan\delta \to min} \quad (2)$$

$$\log\left(\frac{G_N^0}{G_x}\right) = 0.38 + \frac{2.63\log(\frac{M_w}{M_n})}{1+2.45\log(\frac{M_w}{M_n})} \quad (3)$$

The weight average molecular weight $M_w$ and number average molecular weight $M_n$ for the blends were calculated using classic formula in polymer physics [38]:

$$M_w = w_1 M_{w1} + w_2 M_{w2} \quad (4)$$

$$\frac{1}{M_n} = \frac{w_1}{M_{n1}} + \frac{w_2}{M_{n2}} \quad (5)$$

in which $w$ is the weight fraction and subscripts 1 and 2 refer to blend components 1 and 2, respectively. The plateau modulus $G_N^0$ calculated by eq 2, the crossover modulus $G_x$ and $M_e$ calculated by MIN method and crossover modulus-based method of the PMMA/SMA blend films cast from different mixed solvents are presented in Fig. 3. It can be seen that $G_N^0$ decreases and $M_e$ increases as the mass ratio of acetic acid increases, indicating a entanglement depression in the resultant blend films. Furthermore, as mentioned in Experimental section, the $G_{N\,exp}^0$ and $G_x$ in the inset of Figure 3 were obtained at the higher frequency than 0.1 rad/s, which means that these moduli data for calculating are equilibrium value (indicated by Fig. S3 in Supporting Information) and the the influence of hot-compression procedure can be ignored.

As well known, the conformation of polymer chains in solution is significantly influenced by the quality of solvent. As mentioned previously, due to the rapid evaporation of the solvent, some chain conformation in the solution will survive in the resultant films. Hence, molecular entanglement and chain conformation in the blend films are closely related to the quality of casting solvent. The solubility parameter $\delta$ of PMMA and SMA is 9.0~9.5 and 8.7~9.1 $cal^{1/2}\cdot cm^{-3/2}$, respectively, while $\delta$ of m-xylene and acetic acid is 8.8 and 12.6 $cal^{1/2}\cdot cm^{-3/2}$, respectively. The $\delta$ of mixed solvent can be calculated by using eq 6 [38], in which $\phi$ is the volume fraction and subscripts 1 and 2 refer to solvent components 1 and 2, respectively.

$$\delta_{mix} = \phi_1\delta_1 + \phi_2\delta_2 \quad (6)$$

As is calculated using eq 6, the $\delta$ of casting solvents with different $R_{ac}$ (0, 0.1, 0.2, 0.4) are 8.8, 9.1, 9.4 and 10.1 $cal^{1/2}\cdot cm^{-3/2}$, respectively. Obviously, the $\Delta\delta$ between the mixed solvents and PMMA/SMA blends changed little as $R_{ac}$ increased, indicating that in principle all of the casting solvents are near good solvent for this blend. In spite of this, the differences among the solvents with different $R_{ac}$ are undeniable for the different $\delta_h$ and $\delta_p$, which represent the contribution of hydrogen bonding and polar force in the three-dimensional solubility parameter, respectively [46]. The $\delta_p$ of PMMA, m-xylene and acetic acid are 4.0, 0.5 and 3.9 $cal^{1/2}\cdot cm^{-3/2}$, while the $\delta_h$ are 3.3, 1.5 and 6.6 $cal^{1/2}\cdot cm^{-3/2}$, respectively [46]. Similarly, $\delta_p$ and $\delta_h$ of the mixed solvents can be obtained according to eq 6. As $R_{ac}$ increases, $\delta_p$ and $\delta_h$ of the mixed solvents calculated using eq 6 generally get close to that of PMMA, meaning the hydrogen bonding and polar force between PMMA chains and the solvents become

stronger. As a result, the PMMA chains spread loosely in solvent with increasing $R_{ac}$ and the segmental alignment brings a local reduction of chain. It's documented that the PMMA chains and SMA chains are likely to entangle with themselves rather than each other owing to their dissimilar chain structure [43, 47]. Hence, most of the topological entanglements happen in the two components themselves. In the mixed solvents with higher $R_{ac}$, less entanglement points are formed in the solution owing to the more loose chain conformation. Therefore, the topological entanglement density decreases with the increase of $R_{ac}$ in the resultant films due to the chain memory effect.

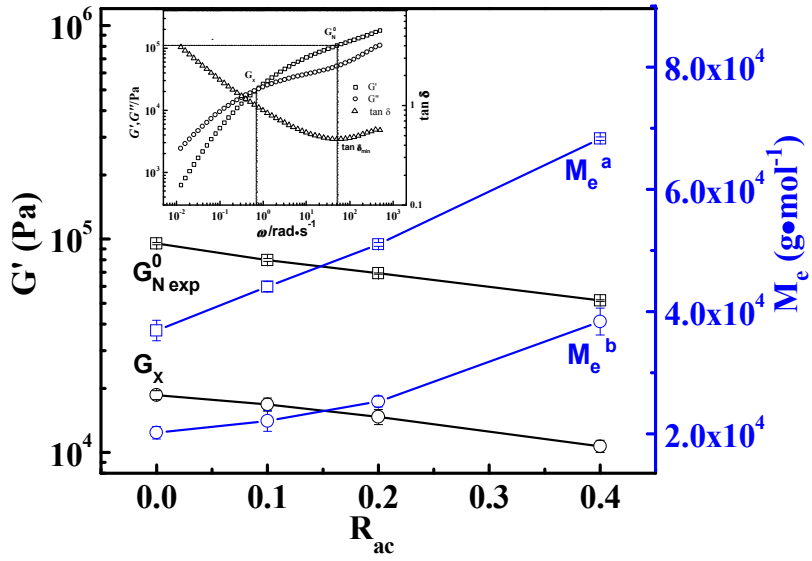


Fig. 3 Plateau modulus $G^0_{N\,exp}$, crossover modulus $G_x$ and entanglement molecular weight estimated using the 'MIN method' ($M_e{}^a$) and the 'Crossover modulus-based' method ($M_e{}^b$) for PMMA/SMA (20/80) blend films cast from solvents with different $R_{ac}$. The inlay presents the dependence of $G'$ , $G''$ and tanδ on frequency for PMMA/SMA(20/80) blend film cast from m-xylene at 160 °C, while the plateau modulus $G^0_{N\,exp}$ and crossover modulus $G_x$ are determined using the 'MIN method' and the 'crossover modulus-based' method, respectively.

### *3.3. Glass transition temperature and cohesional entanglement of molecules*

In order to clarify the influence of architecture structure on glass transition, $T_g$s of the resultant films cast from solvents with different $R_{ac}$ were detected by the broadband dielectric spectroscopy (BDS), which is based on the interaction of an external field with the electric dipole moment of the sample and consequently has been widely employed in a wide variety of scientific fields such as fuel cell testing, molecular interaction, and microstructural characterization. Fig. 4 shows $T_g$s as a function of $R_{ac}$ for PMMA/SMA blend films by BDS measurements. One can find that $T_g$ increases with increasing the mass ratio of acetic acid. Usually, the glass transition behavior of polymer film can be influenced by some factors such as chain entanglement [5], substrate [48], interfacial conditions [49], film thickness [50] and residual solvents [51-53]. In this investigation, the influences of substrate, interfacial conditions, film thickness and residual solvents can be ignored because all the experiment conditions are uniform and the residual solvents are removed completely. Note that in most cases reported previously, the elevated $T_g$ is related to the increased entanglement degree [5, 7, 19, 54, 55]. In previous study [19], the $T_g$ of PMMA/SMA blends increases when annealing time or temperature increases owing to the increased topological entanglement density during the annealing process. Therefore, the $T_g$ should be positive correlated with the topological entanglement density. Considering the decreased topological entanglement density in PMMA/SMA films with the increase of $R_{ac}$ as mentioned in last section, this phenomenon that $T_g$ increases as the extent of chain entanglement decreases is rather interesting. Lu et al. found that a hydrophilic polymer polyacrylamide (PAL) presented an increased $T_g$ with decreasing

chain entanglement and they attributed it to the strong molecular interaction formed between an amino group and a carbonyl group in PAL [56]. However, the PMMA/SMA system differs from the PAL one. It is a hydrophobic one and there is no intermolecular interaction between PMMA and SMA molecular, because the hydrogen bonding only occurs between the polymer and the casting solvents during sample preparation.

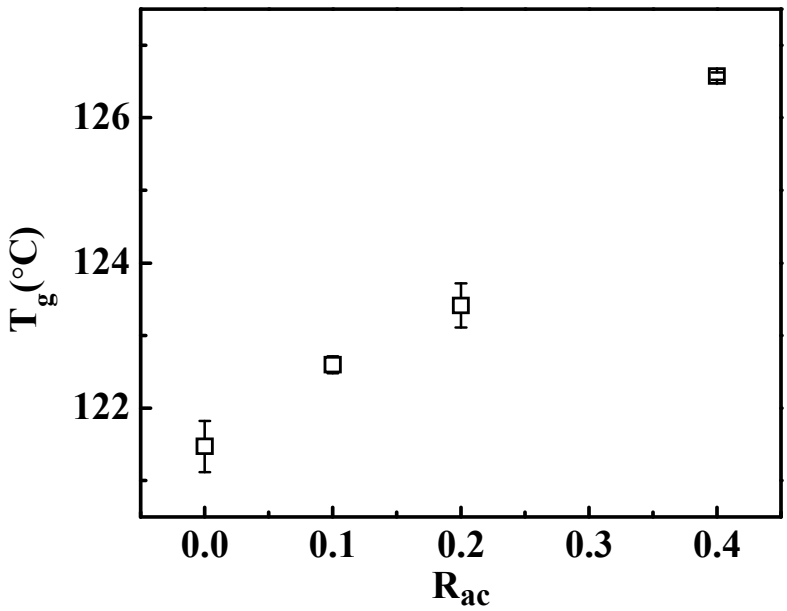


Fig. 4 $T_g$s of PMMA/SMA (20/80) blend films cast from solvents with different $R_{ac}$ measured by broadband dielectric spectroscopy with a heating rate of 3 °C/min at 10 Hz.

To explore the reason of elevated $T_g$ in PMMA/SMA films cast from the mixed solvents with $R_{ac}$, the cohesional entanglements in polymers mentioned above was investigated. Previously, some evidences of cohesional entanglements have been demonstrated by low wavevector wide angle neutron scattering [57], wide angle X-ray scattering [58], high resolution solid state NMR experiments [59] and DSC

[27]. Fig.5 gives the reversing and non-reversing heat flows of PMMA/SMA blend films obtained by modulated DSC test. The reversing signal presenting glass transition shifts towards higher temperature with increasing $R_{ac}$. It is observed that $T_g$ obtained from MDSC is lower than that measured by BDS for each sample, but its variation trend with $R_{ac}$ is in good accord with the BDS result in Fig.4. These $T_g$ differences obtained from two methods should result from the different testing principle. On the other hand, there is only one non-reversing heat flow signal at 109.1 $^{o}$C when the casting solvent is pure m-xylene, while another signal at about 116 $^{o}$C appears at higher temperature when hydrogen bonding exists between PMMA/SMA and casting solvents. With the increasing of $R_{ac}$, the signal at lower temperature weakens and the one at higher temperature becomes stronger. The double-peak behavior has been found in many systems [60-63], and one considers that the temperature endothermic peak located in physically aged poly(DL-lactide) is induced by the disengaging of the cohesional entanglements formed during physical aging [63]. In this investigation, it is noted for the blend sample prepared by pure m-xylene, its $T_g$ is about 112.1 $^{o}$C and it is slightly higher than the peak temperature of 109.1$^{o}$C on the non-reversing heat flow curve. This endothermic peak at 109.1 $^{o}$C should present the energy barrier acquired of segment motion, which may induce by various Van der waals interaction in these polymers including cohesional entanglement. For the blend samples prepared by various mixed solvents, the endothermic peak at about 116 $^{o}$C indicates that a greater energy barrier which segment motion must overcome. With increasing $R_{ac}$, the endothermic peak at about 109 $^{o}$C decreases and the one at

about 116 °C becomes stronger, so $T_g$s of these blends gradually rise. Thus, these results clearly show that the endothermic peak at about 116 °C in PMMA/SMA blend films should be ascribed to the cohesional entanglements induced by hydrogen bonding between the polymer and the casting solvents. The enhanced signal at high temperature indicates an increasing quantity of cohesional entanglements with increasing $R_{ac}$.

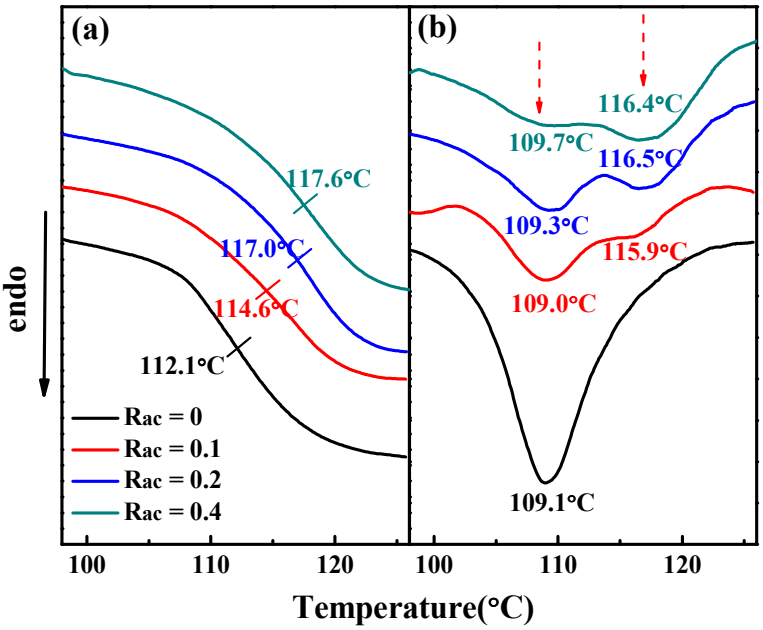


Fig. 5 Variation of reversing (a) and non-reversing (b) heat flow with temperature for PMMA/SMA (20/80) blend films cast from solvents with different $R_{ac}$ measured by MDSC upon heating.

As discussed previously, in the blends/mixed solvent solutions, the hydrogen bonding and polar force between PMMA chains and the solvents become stronger with increasing $R_{ac}$, hence the PMMA chains spread loosely and more segmental alignment appears. Furthermore, there are more opportunities for local parallel alignment neighboring segments to form cohesional entanglements in the

cast-solution with increasing $R_{ac}$. Due to the memory effect, the amount of the cohesional entanglements in the resultant blend films may also increase as $R_{ac}$ increases. It was reported that the average cohesional entanglement spacing along the chain was much smaller than that of the topological entanglement below $T_g$, and the cohesional entanglements prevented the occurrence of the long-range cooperative conformational changes of the chain and the polymers presented a glassy state [26]. As the $R_{ac}$ increases, the cohesional entanglement spacing along the chains become smaller, so a higher temperature is acquired to offer a sufficient energy for the polymer segments to overcome the baffle of cohesional entanglements. During heating, the cohesional entanglements will gradually disentangle or vanish, so the long-range cooperative motions are unlocked. Once the temperature reaches $T_g$, the cohesional entanglement spacing is large enough for rubber elasticity and consequently the cooperative changes of conformation involving successive backbone bonds are permitted [26]. Hence, even the topological entanglement density decreases in samples cast from mixed solvents with higher $R_{ac}$, $T_g$ increases due to the incremental cohesional entanglement, which might be destroyed during the high temperature rheological tests at 160 $^{o}$C. In accord with the previous study [45], the cohesional entanglements are indeed important to the physical properties of polymers near $T_g$ and in their glassy state. Furthermore, as discussed above, the cohesional entanglement could be destroyed partially when the temperature exceeds the $T_g$. Since the experiments in Figure 3 were conducted at 160$^{o}$C, at which most of the cohesional entanglement would be destroyed, consequently the contribution of

cohesional entanglement to the plateau modulus can almost be ignored.

In addition, it needs to be pointed out that a fixed sample preparation condition including concentration and casting method was chosen in order to make a reliable comparison between experimental results. Furthermore, to obtain reliable experimental results and conclusion, PMMA/SMA blends with other different composition were also investigated. It is found that the experimental results of these samples are rather similar to those of PMMA/SMA with composition of 20/80, as indicated by Fig. S5 and Fig. S6 in Supporting Information.

### *3.4. Molecular dynamics*

#### *3.4.1. α-relaxation process*

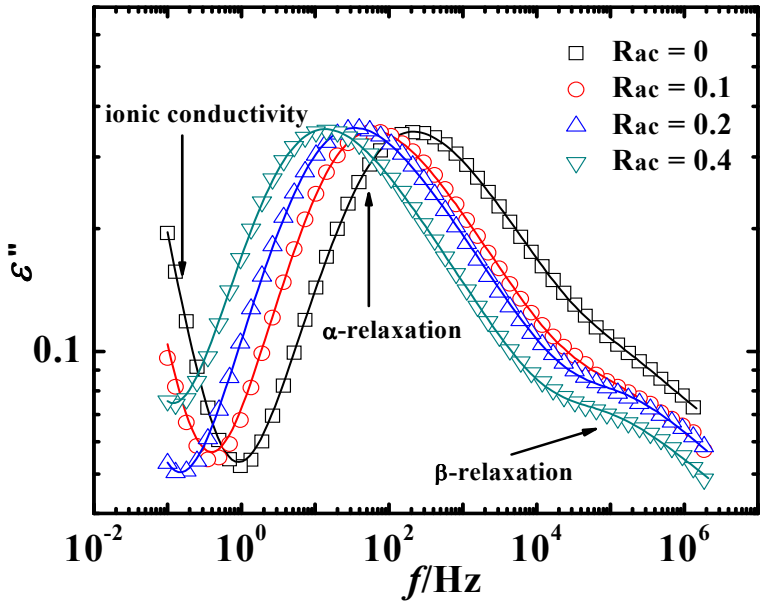


Fig. 6 Dielectric loss ε" as a function of frequency for PMMA/SMA (20/80) blend films cast from mixed solvents with different mass ratio of acetic acid at 130 °C. The solid curves represent HN fittings of the data.

Usually, molecular dynamics is directly influenced by the chain entanglement. In

order to investigate the effect of hydrogen bonding between polymer/solvent on molecular structure of the resultant films, the molecular dynamics of PMMA/SMA films was examined. Fig. 6 demonstrates the frequency dependences of dielectric loss $\varepsilon''$ for PMMA/SMA (20/80) blend films cast from the pure m-xylene and mixed solvents at a weight concentration of 5% at 130 $^{o}$C. In the frequency range investigated herein, three processes can be observed, namely ionic conductivity, $\alpha$- and $\beta$-relaxation from low to high frequency, respectively. Similar to the polyurethane/styrene-acrylonitrile system [64], the process of ionic conductivity is attributed to the accumulation of charge carriers at the interface between PMMA and SMA segments phase. The $\alpha$-relaxation is related to the segment motion of the blends and the $\beta$-relaxation corresponds to the partial rotation or conformational changes of the $-COOCH_3$ side groups around the C-C bond on the backbone of the PMMA component [39]. In order to acquire more quantitative Information, the dielectric loss of the complex dielectric function was analyzed according to the Havriliak-Negami (HN) equation (eq. 7). It can be seen that the HN equation agrees well with the experimental data [65].

$$\varepsilon^* = \varepsilon_\infty + \frac{\Delta\varepsilon}{[1+(i\omega\tau_{HN})^{\alpha_{HN}}]^{\beta_{HN}}} - i\frac{\sigma}{\varepsilon_0\omega^s} \quad (7)$$

in which $\omega$ is angular frequency ( $\omega = 2\pi f$ ), $\varepsilon^*$ is the complex dielectric constant, $\varepsilon_0$ and $\varepsilon_\infty$ is dielectric permittivity of vacuum and the unrelaxed ($\omega = \infty$) value of the dielectric constant respectively, $\Delta\varepsilon$ is the dielectric strength, and $\tau_{HN}$ is the HN

characteristic relaxation time. The exponents $\alpha_{HN}$ and $\beta_{HN}$ ($0<\alpha_{HN}, \beta_{HN} \leq 1$) are shape parameters which describe the symmetric and asymmetric broadening of the relaxation time distribution, respectively. Here, the $i\frac{\sigma}{\varepsilon_0 \omega^s}$ presents the process of ionic conductivity, in which $\sigma$ is the dc conductivity constant, $\varepsilon_0$ is the dielectric permittivity of vacuum and $s$ ($0 < s < 1$) is a coefficient characterizing the conduction mechanism. In this work, two HN functions and a conductivity process were used to analyze the isothermal dielectric spectra. Furthermore, $\tau_{HN}$ is related to $\tau_{max}$ corresponding to the maximum of the dielectric loss by eq. 8 [65].

$$\tau_{max} = \tau_{HN}\left(sin\frac{\alpha_{HN}\beta_{HN}\pi}{2(\beta_{HN}+1)}\right)^{\frac{1}{\alpha_{HN}}}\left(sin\frac{\alpha_{HN}\pi}{2(\beta_{HN}+1)}\right)^{-1/\alpha_{HN}} \quad (8)$$

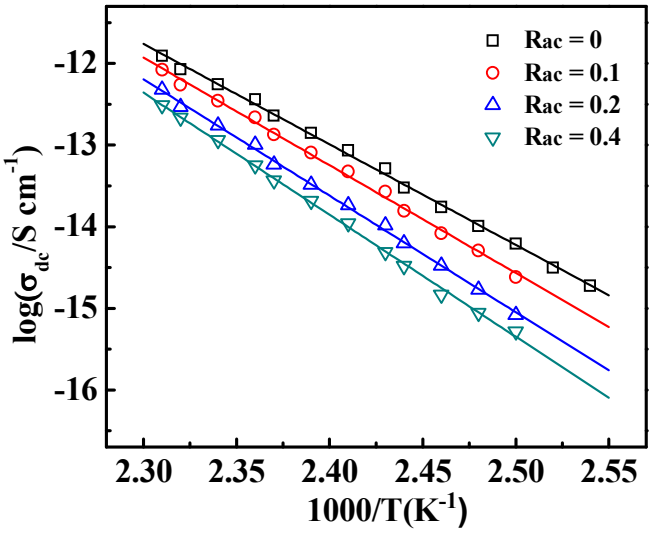


Fig. 7 Dependence of dc conductivity on temperature for PMMA/SMA (20/80) blend films cast from mixed solvents with various $R_{ac}$ at a concentration of 5wt%. The solid curves represent Arrhenius fittings of the data.

In Fig. 6, the ionic conductivity processes of the resultant films are obviously distinct. To further understand the effect of hydrogen bonding between solvent and polymer on dc conductivity of the resultant films, dc conductivity were obtained by fitting raw data in Fig.6 using eq.7. Fig. 7 shows the dependences of dc conductivity on temperature for PMMA/SMA (20/80) blend films cast from mixed solvents with difference $R_{ac}$ and the lines fitted by Arrhenius equation. It can be seen that $\sigma$ of a given sample increases with increasing temperature, indicating that the ionic conduction process is strengthened at elevated temperatures. It can be explained by the increased mobility of ions at elevated temperatures and the enhanced wagging vibration of molecular framework and side chains, as indicated by Ref 66. Furthermore, there is no sharp change of the dc conductivity, meaning that no phase transition process happens in the temperature range investigated. Compared with the blend films cast from pure m-xylene, the dc conductivity of samples cast from mixed solvents is lower. The conductivity activation energy can be obtained by Arrhenius equation fitting, which is assumed to be the energy required to move the ion in the ionic conductivity process. The activation energy values of different samples cast from different solvents ($R_{ac}$ = 0, 0.1, 0.2, 0.4) are 102.39±2.6, 109.74±3.8, 118.66 ±3.1and 124.30±3.2 kJ • $mol^{-1}$, respectively. As the mass ratio of acetic acid in the mixed solvent increases, the increasing activation energy suggests it is more difficult for the casting films to be conductive. It implies a more uniform structure in the blend films cast from the mixed solvents due to the more homogeneous solution system. In our previous work [14], it was found that PMMA/SMA blend film cast from DMF

552 could present a higher $\sigma_{dc}$ than that from chloroform, MEK and THF. If the hydrogen
553 bonding between PMMA and DMF plays an important role in the solution, the
554 PMMA/SMA chains should spread more homogeneous and the resultant film is more
555 uniform, as a result，a lower $\sigma_{dc}$ than films cast from other solvents will appear.
556 However, the fact is opposite to the assumption. Therefore, in spite of the hydrogen
557 bonding between PMMA and DMF [3], the extraordinary performance of films cast
558 from DMF may result from the poor solvent property of DMF rather than the
559 interaction between PMMA and DMF.

560 Fig. 8 shows $\tau_{max}$ of the $\alpha$-relaxation as a function of temperature for PMMA/SMA
561 (20/80) blend films cast from m-xylene and mixed solvents with various $R_{ac}$.
562 Meanwhile, the normalized $\varepsilon''$ of different blend films at 130 $^{o}$C is presented in the
563 inlay. It can be observed that the $\alpha$-relaxation peak shifts towards lower frequency
564 and $\tau_{max}$ increases with the increase of $R_{ac}$, indicating the decreased segmental motion
565 ability. These phenomena are similar to those for annealed films or films cast from
566 solutions with higher concentration in which a higher entanglement density and a
567 more compact chain conformation of polymer chains appears [14, 19]. According to
568 the data of entanglement density reported previously, both the annealing process and
569 larger solution concentration lead to a higher degree of topological entanglement
570 estimated by plateau modulus acquired in rheological tests, which is positive related
571 to the increasing $\tau_{max}$ of α-relaxation. However, the increasing $\tau_{max}$ of α-relaxation
572 demonstrated in Fig. 8 does not correspond with the decreasing topological
573 entanglement density, which can be explained by the increasing cohesional

entanglement. As discussed before, taking the topological entanglement results estimated from Fig. 3 and the cohesional entanglement results obtained by Fig. 5, the average cohesional entanglement spacing along the chain is much smaller than that of the topological entanglement below $T_g$ and the cohesional entanglement might play a more important role than topological entanglement near and below $T_g$ [26, 27]. The increasing cohesional entanglements in the resultant films with increasing $R_{ac}$ will restrict the segmental motion more. As a result, the $\tau_{max}$ of the $\alpha$-relaxation increases with increasing $R_{ac}$ in spite of the decreasing topological entanglement degree.

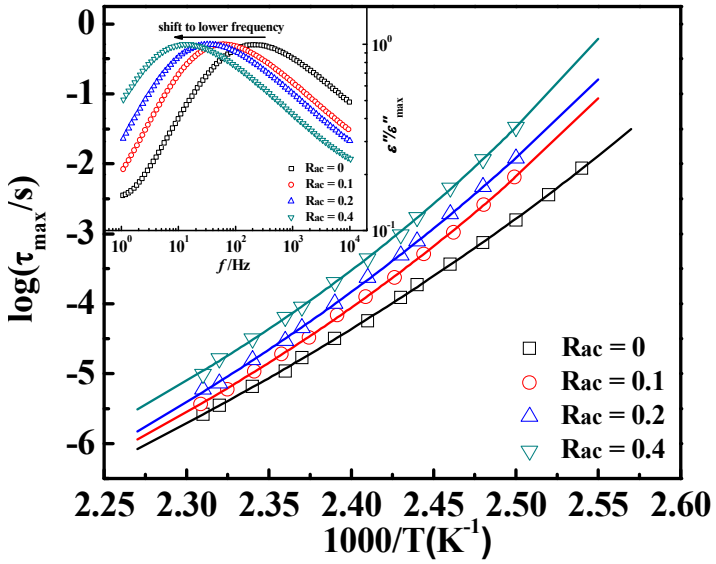


Fig. 8 Relaxation time of the α-relaxation process as a function of temperature for PMMA/SMA (20/80) blend films cast from different solvents at a concentration of 5 wt% measured by BDS. The solid curves represent VFT fittings of the data. The inlays present the corresponding normalized dielectric loss of different PMMA/SMA (20/80) blend films measured at 130 $^{o}$C.

Table1. Relevant fitting parameters for the VFT equation for PMMA/SMA blend films cast from acetic acid/m-xylene mixed solvents with various $R_{ac}$.

| Solvent type | $\log\tau_0$ (s) | $A$(K×10$^3$) | $T_0$(K×10$^2$) |
|---|---|---|---|

| | | | |
|---|---|---|---|
| $R_{ac}$ = 0 | -16.4±0.8 | 1.72±0.21 | 2.73±0.08 |
| $R_{ac}$ = 0.1 | -16.1±1.0 | 1.51±0.24 | 2.93±0.09 |
| $R_{ac}$ = 0.2 | -14.8±0.7 | 1.21±0.16 | 3.04±0.07 |
| $R_{ac}$ = 0.4 | -13.9±0.8 | 1.05±0.15 | 3.15±0.07 |

It is well known that the time-temperature superposition (TTS) principle and equations, *i.e.* Williams-Landel-Ferry (WLF) equation, Vogel-Fulcher-Tamman (VFT) equation and Arrhenius equation have been used in many aspects of polymer physics. However, it is well accepted that the three equations have their own application limitations. WLF equation is valid at the temperatures ranging from $T_g$ to $T_g$+100 $^oC$ for amorphous polymers [67, 68]. And VFT equation equivalent to WLF equation is also applicable to describe the relaxations of segments in glass-forming liquids [69, 70] while Arrhenius equation for whole chain motion and secondary relaxations (β, γ, δ-relaxation)of smaller motion unit than segments [71, 72]. To further understand the segmental dynamics (α-relaxation) of the PMMA/SMA blends with different entanglement states, the VFT equation (eq.9) was used to analyze the temperature dependence of the relaxation time and the curves of fitting data are presented in Fig. 8.

$$log\tau_{max} = log\tau_0 + \frac{A}{T-T_0} \quad (9)$$

Where $\tau_0$ is the relaxation time at infinite temperature, $A$ is a numerical constant related to fragility, and $T_0$ is the so-called Vogel temperature, typically 30~70 K

610 below $T_g$. The parameters obtained from fitting by VFT equation to $\tau_{max}$ in Fig. 8 are
611 listed in Table 1. Obviously, the relaxation time $\tau_0$ and the Vogel temperature $T_0$
612 increases with increasing acetic acid mass ratio in mixed solvents, which is in good
613 agreement with the $T_g$ and $\tau_{max}$ results discussed above. The decreased fragility
614 parameter $A$ indicates an increase of fragility of the PMMA/SMA blend films [73]. In
615 the pure m-xylene solvent, the PMMA/SMA molecular chains spread
616 heterogeneously with curly molecular clews connected by loose chains, which is
617 similar to the polymer chains in poor solvents [74]. Meanwhile, the acetic acid in
618 mixed solvents provides hydrogen bonding with PMMA chains, which makes the
619 PMMA/SMA blends dissolve better and impenetrate more homogeneously. The loose
620 chains linking the clews play a vital role in the PMMA/SMA blend films cast from
621 m-xylene which makes most contribution to the toughness of the system. Considering
622 the more homogenous chain structure in PMMA/SMA blend films cast from mixed
623 solvents and the less loose chains with higher $R_{ac}$, it's intelligible that the
624 PMMA/SMA blend film becomes more fragile with the increasing mass ratio of
625 acetic acid in mixed solvents.
626

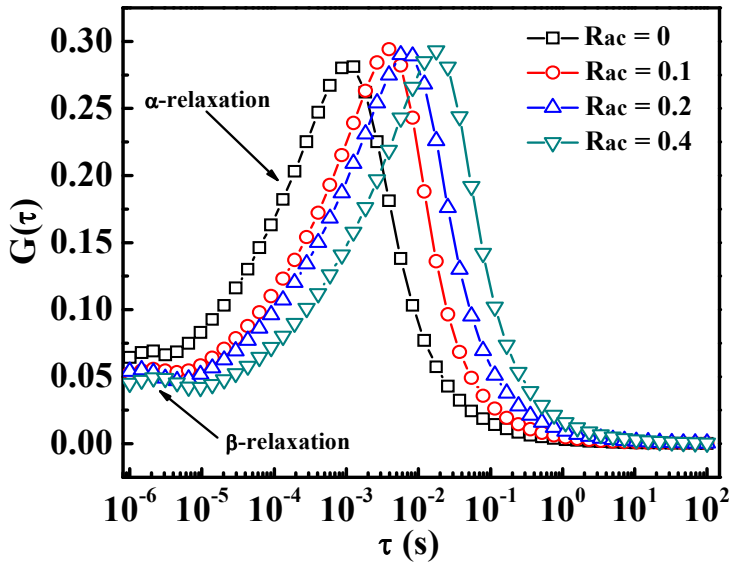


Fig. 9 Relaxation time distribution of PMMA/SMA (20/80) blend films at 130 °C cast from different solvents at a concentration of 5 wt% by BDS.

Furthermore, by analyzing the relaxation time distribution $G(\tau)$ quantitatively, the mechanism of intermolecular interaction between acetic acid and PMMA molecules is revealed. The $G(\tau)$ can be obtained from the following equation[65].

$$G(\tau) = \frac{(\tau/\tau_{HN})^{\alpha\beta}\sin(\beta\theta)}{\pi\tau((\tau/\tau_{HN})^{2\alpha}+2(\tau/\tau_{HN})^{\alpha}\cos(\pi\alpha)+1)^{\frac{\beta}{2}}} \quad (10)$$

In which

$$\theta = \arctan\left(\frac{\sin(\pi\alpha)}{(\tau/\tau_{HN})^{\alpha}+\cos(\pi\alpha)}\right)$$

Fig. 9 shows the $G(\tau)$ curves for various PMMA/SMA (20/80) blend films at 130 °C by BDS measurements. There are two different relaxation modes in the investigated temperature and frequency range, namely, the $\alpha$-relaxation at a longer relaxation timescale and $\beta$-relaxation at the shorter one. As shown in Fig. 9, the $\alpha$-relaxation peak shifts towards longer average relaxation time with increasing $R_{ac}$, indicating an increase of $\alpha$-relaxation time. In despite of $G(\tau)$ shifts towards longer

relaxation time, no obvious distribution broadening of the $\alpha$-relaxation is observed. It means that the heterogeneity of the segmental dynamics in the films is hardly influenced by the change of blends architecture and chain entanglement caused by the hydrogen bonding between PMMA and acetic acid. To further discuss the heterogeneity of the segmental dynamics, the shape parameters of $\alpha$-relaxation peaks were also analyzed. The $\alpha_{HN}$ and $\beta_{HN}$ which describe the symmetric and asymmetric broadening of the relaxation time distribution are listed in Table 2. For the films cast from pure m-xylene and mixed solvents with various $R_{ac}$, the values of $\alpha_{HN}$ and $\beta_{HN}$ are close to each other. Hence, the $\alpha$-relaxation width and symmetry are considered to be almost unchanged in PMMA/SMA blend films cast from mixed solvents with different $R_{ac}$.

Table 2 Shape parameters of the α-relaxation at 130 °C for different PMMA/SMA (20/80) blend films cast from solvents with different ratio of acetic acid at the concentration of 5 wt%.

| **Solvent type** | $\alpha_{HN}$ | $\beta_{HN}$ |
|---|---|---|
| $R_{ac}$ = 0 | 0.688±0.008 | 0.455±0.001 |
| $R_{ac}$ = 0.1 | 0.706±0.018 | 0.427±0.007 |
| $R_{ac}$ = 0.2 | 0.697±0.003 | 0.442±0.011 |
| $R_{ac}$ = 0.4 | 0.711±0.001 | 0.425±0.002 |

*β-relaxation process*

In Fig. 9, it is seen that the boundary between $\alpha$- and $\beta$-relaxation time distribution moves to a longer time with increasing $R_{ac}$ in the $G(\tau)$ curves, while the average relaxation time of $\beta$-relaxation is hardly changed. The $\beta$-relaxation of the PMMA/SMA blends reflects the partial rotation or conformational changes of the

663 -$COOCH_3$ side groups around the C-C bond in the main chain of the PMMA
664 component [39]. The $\beta$-relaxation is relatively weak compared with the $\alpha$-relaxation
665 due to the facts that only 20 wt% PMMA in the blends and the $\beta$-relaxation of SMA
666 cannot be observed in temperature and frequency ranges investigated [5]. The
667 average ability of the -$COOCH_3$ to rotate partially or to change the conformation is
668 considered to be unchanged with the increase of $R_{ac}$ on the basis of the unchanged
669 $\beta$-relaxation average distribution time.

670 In order to further investigate the $\beta$-relaxation, frequency sweep at 50 $^{o}$C was
671 carried out. Fig. 10 shows the normalized dielectric loss $\varepsilon''$ as a function of frequency
672 for PMMA/SMA (20/80) blend films. It is seen that the $\beta$-relaxation peaks remain
673 around $10^3$-$10^4$ Hz and little difference appears in the peak positions of blend films
674 cast from mixed solvents with various $R_{ac}$. It declares that the average ability of
675 -$COOCH_3$ in PMMA molecular to rotate or to change its conformation will not be
676 affected by the variation in architecture in the films cast from different mixed
677 solvents. In other words, the hydrogen bonding between solvents and PMMA hardly
678 affects the average mobility of -$COOCH_3$ in resultant blend films. With the increase
679 of $R_{ac}$, the boundary between $\alpha$- and $\beta$-relaxation moves towards lower frequency,
680 which corresponds to the $G(\tau)$ curves in Fig. 9. This may be ascribed to the shift of
681 the $\alpha$-relaxation with increasing $R_{ac}$, so the merged boundary of $\alpha$- and $\beta$-relaxation
682 shifts accordingly. In fact, besides the average mobility of -$COOCH_3$, the
683 homogeneity of $\beta$-relaxation is almost unchanged because the peaks in the
684 normalized curves coincide. Above all, neither the dynamics nor the distribution of

685 $\beta$-relaxation in solvent-cast PMMA/SMA films is influenced by the hydrogen
686 bonding between solvent and polymer chains, indicating that the local environment of
687 the segments is not changed.

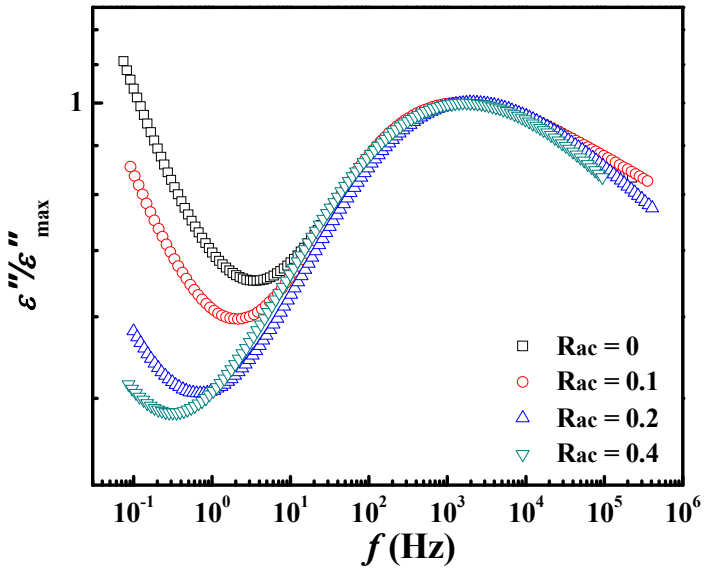


688

689 Fig. 10 Normalized frequency-dependence of dielectric loss $\varepsilon$'' for PMMA/SMA (20/80) blend
690 films cast from mixed solvents with different $R_{ac}$ at 50 °C.

691

692 ## 4. Conclusion

693 The hydrogen bonding between PMMA and acetic acid during casting film has a
694 distinct effect on the molecular architecture of PMMA/SMA in solutions, which can
695 lead to the pronounced changes of macroscopic properties and molecular dynamics in
696 the resultant PMMA/SMA blend films. $T_g$ increases and the $\alpha$-relaxation shifts to
697 lower frequency, indicating a pronounced inhibiting effect on segmental dynamics in
698 blend film cast from mixed solvent with increasing hydrogen bonding between
699 PMMA and acetic acid. In mixed solvent with higher $R_{ac}$, there are more

opportunities for the local parallel alignment neighboring segments to form cohesional entanglements. As a result, although the topological entanglement density obtained by rheological measurement decreases, the cohesional entanglement in the film rises as $R_{ac}$ increases, which restricts the segmental motion and plays a vital role in molecular dynamics near $T_g$. The molecular dynamic results obtained from broadband dielectric spectroscopy also confirm the role of cohesional entanglement. The dc conductivity decreases due to the more uniform structure in PMMA/SMA (20/80) blend film with increasing $R_{ac}$ while the width distribution of $\alpha$-relaxation nor the dynamics of $\beta$-relaxation in these films is influenced by hydrogen bonding since the unchanged local environment of the segments.

## Acknowledgments

This work was supported by the National Nature Science Foundation of China (No. 51173165 and 51173157), the Nature Science Foundation of Zhejiang Province (No.Y4100314) and the Fundamental Research Funds for the Central Universities (no. 2013QNA4048).

## References

1 T. Wang, A. D. F. Dunbar, P. A. Staniec, A. J. Pearson, P. E. Hopkinson, J. E. MacDonald, S. Lilliu, C. Pizzey, N. J. Terrill, A. M. Donald, A. J. Ryan, R. A. L. Jones and D. G. Lidzey, *Soft Matter*, 2010, **6**, 4128.

2 A. Diethert, E. Metwalli, R. Meier, Q. Zhong, R. A. Campbell, R. Cubitt and P.

Mueller-Buschbaum, *Soft Matter*, 2011, **7**, 6648.
3 N. Patra, A. Barone and M. Salerno, *Adv. Polym. Tech.*, 2011, **30**, 12.
4 M. Wadey, I. Hsieh, K. Cavicchi and S. Cheng, *Macromolecules*, 2012, **45**, 5538.
5 Y. Lin, Y. G. Shangguan, M. Zuo, E. Harkin-Jones and Q. Zheng, *Polymer*, 2012, **53**, 1418.
6 R. N. Li, A. Clough, Z. H. Yang and O. K. C. Tsui, *Macromolecules*, 2012, **45**, 1085.
7 W. R. Rong, Z. Y. Fan, Y. Yu, H. S. Bu and M. Wang, *J. Polym. Sci., Part B: Polym. Phys.*, 2005, **43**, 2243.
8 A. A. Mansour, S. A. Madbouly, G. Hohne and W. Dollhopf, *Polym. Int.*, 1997, **42**, 143.
9 R. O. Sirotkin and N. W. Brooks, *Polymer*, 2001, **42**, 9801.
10 P. Rojanapitayakorn, S. Thongyai, J. S. Higgins and N. Clarke, *Polymer*, 2001, **42**, 3475.
11 X. H. Wang, R. G. Liu, M. Wu, Z. G. Wang and Y. Huang, *Polymer*, 2009, **50**, 5824.
12 Y. G. Shangguan, L. Zhao, L. Tao and Q. Zheng, *J. Polym. Sci. Pol. Phys.*, 2007, **45**, 1704.
13 R. c, S. Ata, K. Kuboyama and T. Ougizawa, *J. Appl. Polym. Sci.*, 2013, **128**, 60.
14 Y. Lin, Y. Q. Tan, B. W. Qiu, J. Q. Cheng, W. J. Wang, Y. G. Shangguan and Q. Zheng, *J. Membrane Sci.*, 2013, **439**, 20.
15 H. L. Lin, Y. C. Chen, C. C. Li, C. P. Cheng and T. L. Yu, *J. Power Sources*, 2008, **181**, 228-236.
16 M. S. Jun, Y. W. Choi and J. D. Kim, *J. Membrane Sci.*, 2012, **396**, 32.
17 D. Xue, X. Wang, H. Ni, W. Zhang and G. Xue, *Langmuir*, 2009, **25**, 2248.
18 X. Wang, H. Ni, D. Xue, X. Wang, R. Feng and H. Wang, *J. Colloid Interface Sci.*, 2008, **321**, 373.
19 Y. Lin, Y. Q. Tan, B. W. Qiu, Y. G. Shangguan, E. Harkin-Jones and Q. Zheng, *J. Phys. Chem. B*, 2013, **117**, 697.
20 K. Iwata, *J. Phys. Soc. Jpn.*, 1974, **37**, 1413.
21 K. Iwata, *J. Phys. Soc. Jpn.*, 1974, **37**, 1423.
22 K. Iwata, *J. Phys. Soc. Jpn.*, 1974, **37**, 1429.
23 S. Batten and R. Robson, *Angew. Chem. Int. Ed.*, 1998, **37**, 1460.
24 E. Donth, M. Beiner, S. Reissig, J. Korus, F. Garwe, S. Vieweg, S. Kahle, E. Hempel and K. Schroter, *Macromolecules*, 1996, **29**, 6589.
25 R. Y. Qian, China-U.K Bilateral Conference on Polymer Science, Beijing, 1992.
26 R. Y. Qian, L. H. Wu, D. Y. Shen, D. H. Napper, R. A. Mann and D. F. Sangster, *Macromolecules*, 1993, **26**, 2950.
27 R. Qian, *Macromol. Symp.*, 1997, **124**, 15.
28 X. Tian, X. Jiang, B. Zhu and Y. Xu, *J. Membrane Sci.*, 2006, **279**, 479.
29 J. Huang, X. Li and Q. Guo, *Eur. Polym. J.*, 1997, **33**, 659.
30 Z. Xu, H. Tsai, H. Wang and M. Cotlet, *J. Phys. Chem. B*, 2010, **114**, 11746.
31 C. Chiang, S. Chen and C. Wu, *Org. Electron.*, 2013, **14**, 2369.
32 K. Song, J. Lee, H. Kim, D. Kim, S. Kim and C. Kim, *Synth. Met.*, 2000, **110**, 57.
33 K. Thomas, A. Chenneviere, G. Reiter and U. Steiner, *Phys. Rev. E*, 2011, **83**.
34 P. Chen, A. Rassamesard, H. Chen and S. Chen, *Macromolecules*, 2013, **46**, 5657.
35 E. Cadogan, C. Lee, S. Popuri and H. Lin, *Int. J. Polym. Mater.*, 2014, **63**, 708.
36 R. Wang and Z. G. Wang, *Macromolecules*, **2014**, **47**, 4094.
37 J. H. Hildebrand, J. M. Prausnitz and R. L. Scott, *Regular and related solutions : the solubility of gases, liquids, and solids*, Van Nostrand Reinhold, New York ; London, 1970.
38 M. Rubinstein and R. Colby, *Polymers Physics*, Oxford, 2003.

39 R. Bergman, F. Alvarez, A. Alegria and J. Colmenero, *J. Chem. Phys.*, 1998, **109**, 7546.
40 J. L. Viovy, *Electrophoresis*, 1993, **14**, 1088.
41 D. Broseta, L. Leibler, A. Lapp and C. Strazielle, *Europhys. Lett.*, 1986, **2**, 733.
42 C. Heller, *J. Chromatogr. A*, 1995, **698**, 19.
43 S. H. Wu, *J. Polym. Sci., Part B: Polym. Phys.*, 1987, **25**, 557.
44 S. H. Wu, *J. Polym. Sci., Part B: Polym. Phys.*, 1989, **27**, 723.
45 S. H. Wu and R. Beckerbauer, *Polymer*, 1992, **33**, 509.
46 C. M. Hansen, *The three dimensional solubility parameter and solvent diffusion coefficient : Their importance in surface coating formalation*, Danish Technical Press, Copenhagen, 1967.
47 S. H. Wu, *Polymer*, 1987, **28**, 1144.
48 M. Erber, M. Tress, E. Mapesa, A. Serghei, K. Eichhorn, B. Voit and F. Kremer, *Macromolecules*, 2010, **43**, 7729.
49 A. Serghei, M. Tress and F. Kremer, *J. Chem. Phys.*, 2009, **131**.
50 D. Fryer, R. Peters, E. Kim, J. Tomaszewski, J. de Pablo, P. Nealey, C. White and W. Wu, *Macromolecules*, 2001, **34**, 5627.
51 W. Zheng and S. Simon, *Polymer*, 2006, **47**, 3520.
52 C. Gourgon, J. Tortai, F. Lazzarino, C. Perret, G. Micouin, O. Joubert and S. Landis, *J. Vac. Sci. Technol.,B,* 2004, **22**, 602.
53 C. Witschi and E. Doelker, *Eur. J.Pharm. Biopharm.*, 1997, **43**, 215.
54 S. M. Aharoni, *Polym. Adv. Technol.*, 1998, **9**, 169.
55 D. H. Huang, Y. M. Yang, G. Q. Zhuang and B. Y. Li, *Macromolecules*, 2000, **33**, 461.
56 X. Lu, G. Xue and Y. Mi, *J. Appl. Polym. Sci.*, 2011, **119**, 2310.
57 L. Cervinka, E. Fischer, K. Hahn, B. Jiang, G. Hellmann and K. Kuhn, *Polymer*, 1987, **28**, 1287.
58 G. Mitchell, *Polymer*, 1984, **25**, 1562.
59 H. Feng, Z. Feng, H. Ruan and L. Shen, *Macromolecules*, 1992, **25**, 5981.
60 P. Lindenmeyer, *Polym. Eng. Sci.*, 1981, **21**, 958..
61 S. Lee, H. Miyaji and P. Geil, *J. Macromol. Sci., Phys.*, 1983, **B22**, 489.
62 D. Hourston, M. Song, A. Hammiche, H. Pollock and M. Reading, *Polymer*, 1996, **37**, 243.
63 K. Liao, D. Quan and Z. Lu, *Eur. Polym. J.*, 2002, **38**, 157.
64 A. Kanapitsas, P. Pissis and A. G. Estrella, *Eur. Polym. J.*, 1999, **35**, 923.
65 Havrilia.S and S. Negami, *Polymer*, 1967, **8**, 161.
66 H. S. S. Jois and D. K. Bhat, *J. Appl. Polym. Sci.*, 2013, **130**, 3074.
67 M. L. Williams, R. F. Landel, J. D. Ferry, *J. Am. Chem. Soc.,* 1955*,* **77**, 3701.
68 J. D. Ferry, *Viscoelastic properties of polymers*, John Wiley & Sons, 1980.
69 F. Stickel, E. W. Fischer, and R. Richert, *J. Chem. Phys.,* 1995, **102**, 6251.
70 J. F. Mano, E. Pereira, *J. Phys. Chem. A*, 2004*,* **108**, 10824.
71 M. T. Shaw and W. J. MacKnight, *Introduction to Polymer Viscoelasticity*, Wiley, 2005.
72 L. H. Sperling, *Introduction to Physical Polymer Science,* Wiley, 2005.
73 R. Richert and C. A. Angell, *J. Chem. Phys.*, 1998, **108**, 9016.
74 B. J. Briscoe, A. Akram, M. J. Adams, S. A. Johnson and D. M. Gorman, *J. Mater. Sci.*, 2002, **37**, 4929.

# Caption for Figures and Tables

**Fig. 1** Schematical of toplogical entanglement and cohesional entanglement. Reproduced with permission from 1997, Wiley VCH.

**Fig. 2** FTIR spectra of (a) PMMA film cast from acetic acid, acetic acid and PMMA/acetic acid solution, (b) real-time FTIR spectra of PMMA/acetic acid solution as the acetic acid volatilized and (c) PMMA films cast from acetic acid, m-xylene and their mixed solvent, respectively. The four curves in (b) correspond to the time of the marked points (1, 2, 3, 4) in Fig. S4 in Supporting Information.

**Fig. 3** Plateau modulus $G_{N\,exp}^{0}$, crossover modulus $G_x$ and entanglement molecular weight estimated using the 'MIN method' ($M_e{}^a$) and the 'Crossover modulus-based' method ($M_e{}^b$) for PMMA/SMA (20/80) blend films cast from solvents with different $R_{ac}$. The inlay presents the dependence of $G'$ , $G''$ and tanδ on frequency for PMMA/SMA(20/80) blend film cast from m-xylene at 160 °C, while the plateau modulus $G_{N\,exp}^{0}$ and crossover modulus $G_x$ are determined using the 'MIN method' and the 'crossover modulus-based' method, respectively.

**Fig. 4** $T_g$s of PMMA/SMA (20/80) blend films cast from solvents with different $R_{ac}$ measured by the broadband dielectric spectroscopy with a heating rate of 3 °C/min at 10 Hz.

**Fig. 5** Variation of reversing (a) and non-reversing (b) heat flow with temperature for PMMA/SMA (20/80) blend films cast from solvents with different $R_{ac}$. The DSC results were obtained in the modulated mode upon heating with temperature modulation amplitude of 0.5°C and an oscillation period of 60s.

**Fig. 6** Dielectric loss ε" as a function of frequency for PMMA/SMA (20/80) blend films cast from mixed solvents with different mass ratio of acetic acid at 130 °C. The solid curves represent HN fittings of the data.

**Fig. 7** Dependence of dc conductivity on temperature for PMMA/SMA (20/80) blend films cast from mixed solvents with various $R_{ac}$ at a concentration of 5wt%. The solid curves represent Arrhenius fittings of the data.

**Fig. 8** Relaxation time of the α-relaxation process as a function of temperature for PMMA/SMA (20/80) blend films cast from different solvents at a concentration of 5 wt%. The solid curves represent VFT fittings of the data. The inlays present the corresponding normalized dielectric loss of different PMMA/SMA (20/80) blend films measured at 130 °C.

**Fig. 9** Relaxation time distribution of PMMA/SMA (20/80) blend films at 130 °C cast from different solvents at a concentration of 5 wt%.

**Fig. 10** Normalized frequency-dependence of dielectric loss $\varepsilon''$ for PMMA/SMA (20/80) blend films cast from mixed solvents with different $R_{ac}$ at 50 °C.

**Table 1** Relevant fitting parameters for the VFT equation for PMMA/SMA blend films cast from acetic acid/m-xylene mixed solvents with various $R_{ac}$.

**Table 2** Shape parameters of the α-relaxation at 130 °C for different PMMA/SMA (20/80) blend films cast from solvents with different ratio of acetic acid at the concentration of 5 wt%.